Article ID: 1007-7294(2024)12-1970-13

Theoretical and Experimental Research of High-Static-Low-Dynamic Torsional Vibration Isolator for Ship Shafting

LI Lin-tao[1], *LU Jia-zhong*[1], *YANG Zhi-rong*[1], *XIAO Wang-qiang*[2], *RAO Zhu-shi*[3]

(1. School of Marine Engineering, Jimei University, Xiamen 361021, China; 2. School of Aerospace Engineering, Xiamen University, Xiamen 361000, China; 3. State Key laboratory of Mechanical System and Vibration, Shanghai Jiao Tong University, Shanghai 200240, China)

Abstract: High-static-low-dynamic stiffness (HSLDS) vibration isolators have been demonstrated to be an effective means of attenuating low-frequency vibrations, and may be utilized for ship shafting applications to mitigate torsional vibration. This paper presents the construction of a highly compact HSLDS torsional vibration isolator by connecting positive and negative stiffness components in parallel. Based on mechanical model analysis, the restoring torque of negative stiffness components is derived from their springs and connecting rods, while that of positive stiffness components is obtained through their circular section flexible rods. The quasi-zero stiffness characteristics of the HSLDS isolator are achieved through a combination of static structural simulation and experimental test. The torsional vibration isolation performance is assessed by means of numerical simulation and theory analysis. Finally, the frequency-sweep vibration test is conducted. The test results indicate that the HSLDS torsional vibration isolator exhibits superior low-frequency isolation performance compared to its linear counterpart, rendering it a promising solution for mitigating low-frequency torsional vibration in ship shafting.

Key words: ship shafting; high-static-low-dynamic stiffness; torsional vibration isolator

CLC number: U664.21 **Document code:** A **doi:** 10.3969/j.issn.1007-7294.2024.12.012

0 Introduction

Recently, the propeller-shaft-hull coupled vibration and acoustic radiation, as a major source of ship noise, has attracted more and more attention from engineering researchers in the related fields[1]. In addition, the ship's shafting system plays a crucial role in maintaining the propulsion of the vessel, as it may be subjected to unbalance forces or torques that can result in torsional vibrations. A major consideration in the design of ship shafting is the mitigation of vibration and acoustic emissions[2-3], which can pose a threat to ship's safety and stability. When the amplitude of torsional

Received date: 2024-06-17

Foundation item: Supported by the National Natural Science Foundation Project (52475104); Guiding Project of Science and Technology Plan of Fujian Province (2024H0015); Industry-University-Research Joint Innovation Project of Fujian Province (2022H6003) and Leading Innovation Project of China National Nuclear Group (22GFC-JJ12-475)

Biography: LI Lin-tao(1996-), male, master student; YANG Zhi-rong(1981-), male, associate professor, MSc supervisor, corresponding author, E-mail: yzhirong2000@126.com.

vibration exceeds a certain threshold, it may lead to shafting failure, elastic coupling bolt fracture, and localized heating in the shafting system. According to the theory of mechanical vibration[4], it is known that a structure with low stiffness can effectively reduce its natural frequency and thus avoid resonance with external excitation frequencies, achieving effective vibration isolation. However, inadequate stiffness may result in insufficient bearing capacity. Traditionally, achieving a high static torque capacity while isolating low frequency torsional vibration in ship's shafting through elastic coupling has been a challenging task. The HSLD stiffness vibration isolators are rapidly becoming a crucial tool for effectively isolating low-frequency vibrations while simultaneously supporting high static loads[5-6].

In light of the limitations of conventional linear vibration isolators, it is pertinent to undertake theoretical and experimental investigations into the stiffness characteristics of HSLDS vibration isolators. Previous studies have primarily focused on vertical vibration, with relatively less attention given to torsional vibration. Recently, the most common torsional vibration isolator is composed of a positive stiffness element and a negative stiffness element connected in parallel. For instance, Zheng et al[7] devised a torsional isolator featuring HSLD stiffness, wherein the negative stiffness produced by the permanent magnet spring was utilized to counterbalance the positive stiffness supplied by the rubber spring. Zhang et al[8] proposed an HSLDS torsional vibration isolator featuring timely adaptation to load changes, with its positive and negative stiffness provided by spring plates and torsional magnetic springs, respectively. As previously mentioned, vibration isolators utilizing magnetic springs exhibit good low-frequency isolation performance but are susceptible to the influence of current intensity and magnetic fields, resulting in unstable nonlinear stiffness. The application range of magnetic spring isolators is constrained, thus limiting their utility. In order to satisfy the requirements of low-frequency vibration isolation and stable nonlinear stiffness simultaneously, researchers have developed vibration isolators using either structural nonlinearity or material nonlinearity. For example, Zhang et al[9] proposed a torsional isolator with buckling rod deformation that features a simple and compact structure. Zhou et al[10] designed an HSLD stiffness torsional isolator composed of springs, cams, rollers, and vulcanized rubber. Based on this premise, Wang et al[11] substituted vulcanized rubber with torsional springs and investigated the impact of mechanism parameter errors on dynamic stiffness. Liu et al[12] and Wang et al[13] devised a parallel-connected rod spring mechanism to form a torsional vibration isolator, which was verified to exhibit excellent low-frequency isolation performance in terms of dynamic torque transmissibility and power flow. However, the previous research on torsional vibration isolators has not been specifically designed for ship shafting equipment. Further theoretical work is required to investigate the HSLD stiffness characteristics of torsional vibration isolators in the field of ships.

Therefore, the research objective presented in this paper is to design a torsional vibration isolator for ship's shafting with HSLD stiffness characteristics by utilizing parallel connection of spring components with positive and negative stiffness. In this study, with the establishment of a dimensionless model, an analysis of isolator torque transmissibility, simulations and torsional test analyses are conducted to fulfill the dual requirements of transmitting static load torque and isolating low-frequency disturbance torque in shafting systems, thereby enhancing the safety and stability of

such equipment.

1 Structural model of HSLDS torsional vibration isolator

An HSLDS vibration isolator operates on the principle of parallel connection between positive stiffness and negative stiffness. By appropriately selecting negative stiffness components in parallel with positive stiffness components, the resulting stiffness values cancel each other out, leading to a total dynamic stiffness that approaches zero within the static equilibrium position range. This approach effectively reduces natural frequency and achieves low-frequency vibration isolation. In addition, it exhibits high static stiffness at the equilibrium position, thereby endowing the vibration isolation system with an excellent load-bearing capacity. The negative stiffness component of a vibration isolator comprises a spring, connecting rods, and push rods, as depicted in Fig.1(a). In Fig.1(b), a circumferential array of three pairs of springs is shown in the direction of the transmission shaft, where the push rod transmits spring force to the transmission shaft through hinged connecting rods. To ensure the system′s compact and stable structure, as well as consistent stiffness of positive stiffness elements in all directions during torsional vibration, these elements are connected to the transmission shaft via circular section rods arranged axially around a disc. The circular section flexible rods are attached to the isolator shell via a small aperture at one end, and connected in parallel with a negative stiffness element at the other end to form an HSLDS torsional vibration isolator. The physical diagram of the HSLDS torsional vibration isolator, produced through 3D printing technology, is depicted in Fig.1(c). The isolator′s transmission shaft is connected to the driven shaft of the ship′s propulsion system, while its shell is linked to the driving shaft via a flange mechanism.

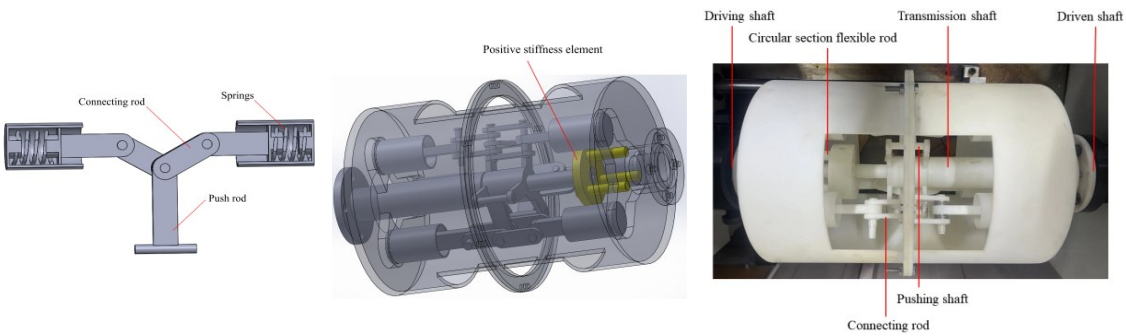

(a) Schematic diagram of negative stiffness element

(b) Schematic diagram of HSLDS isolator

(c) 3D printed physical image of HSLDS isolator.

Fig.1 Structural diagram of HSLD torsional vibration isolator

2 Quasi-zero stiffness characteristic analysis of HSLDS torsional vibration isolator

2.1 Quasi-zero stiffness theory

One end of the circular flexible rod in the positive stiffness element is connected to the shell of

the isolator, and the other end is connected to the transmission shaft. The occurrence of torsional movement will result in a slight angular displacement between the shell and transmission shaft. When viewed axially, one end of the circular flexible rod generates a deflection angle displacement θ around the axis of the other end of the transmission shaft. The deflection w of the deflected end face is from position A to position A', as shown in Fig.2.

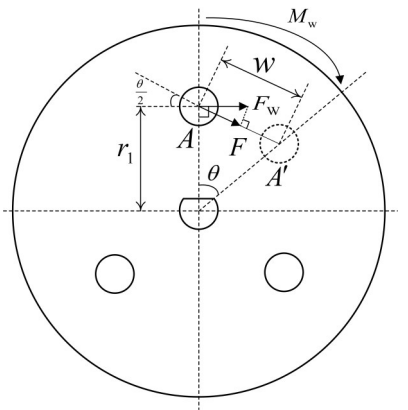

Fig.2 Axial force diagram of flexible rod

When torsional motion occurs, the external input torque M_W, axial deflection w and effective force F_W caused by flexible rod can be expressed as follows:

$$M_W = F_W r_1 \tag{1}$$

$$w = \frac{FL^3}{3EI_P} = \frac{F_W \cos\frac{\theta}{2} L^3}{3EI_P} \tag{2}$$

$$I_P = \frac{\pi d^4}{64} \tag{3}$$

where, L represents the length of flexible rod, E represents the elastic modulus and I_P represents the moment of inertia of the round rod section.

By substituting Eq.(2) and Eq.(3) into Eq.(1), the output torque under static load is equivalent to the external input torque, resulting in the following expression for the output torque:

$$M_r = M_W = \frac{3n_1 E\pi d^4 r_1^2}{32L^3} \tan\frac{\theta}{2} \tag{4}$$

where n_1 and d represent the number and the section diameter of flexible rods respectively while r_1 represents the radial displacement of the flexible rod at the axial deformation end.

The stiffness expression K_r can be obtained by calculating the partial derivative of the output torque M_r with respect to displacement θ.

$$K_r = \frac{3n_1 E\pi d^4 r_1^2}{64L^3} \sec^2\frac{\theta}{2} \tag{5}$$

When the negative stiffness spring is in static balance position, as depicted in Fig.3, the total length of the spring and connecting rod is represented by a, K_S denotes its stiffness, δ indicates its compression, and b denotes the length of the connecting rod.

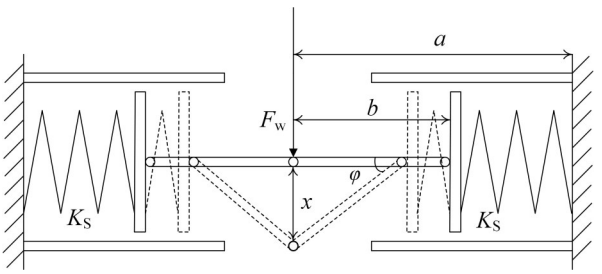

Fig.3 Schematic diagram of rod-spring stress

Once torsional motion occurs, the radial displacement of the shaft under the action of the

torque of the push rod is r_2. The displacement x of the connecting rod is equal to the the length of the connecting rod b multiplied by $\sin\varphi$, and it is also equal to the radial angle displacement θ multiplied by the radial displacement r_2. So the output torque of the spring connecting rod M_S can be given as follows:

$$M_S = 2n_2K_Sr_2^2\theta\left[\frac{L_{S0}-a}{\sqrt{b^2-(r_2\theta)^2}}+1\right] \tag{6}$$

where L_{S0} denotes the original length of the spring.

By adding Eq.(4) and Eq.(6), the torque of negative stiffness connecting-rod paralleling with positive stiffness element can be given as follows:

$$M = M_r + M_S \tag{7}$$

$$M = \frac{3n_1E\pi d^4r_1^2}{32L^3}\tan\frac{\theta}{2} - 2n_2K_Sr_2^2\theta\left[\frac{L_{S0}-a}{\sqrt{b^2-(r_2\theta)^2}}+1\right] \tag{8}$$

Supposing the angular displacement is small, then $\tan\dfrac{\theta}{2}$ can be approximately equal to $\theta/2$ and $\dfrac{3E\pi d^4}{64L^3}$ is the constant coefficient related to the circular flexible rod and can be denoted by K_r, so Eq.(8) can be simplified as follows:

$$M = n_1K_rr_1^2\theta - 2n_2K_Sr_2^2\theta\left[\frac{L_{S0}-a}{\sqrt{b^2-(r_2\theta)^2}}+1\right] \tag{9}$$

Eq.(9) of torque can be non-dimensionalized by introducing the following constants and variables: $\dfrac{M}{n_1K_rr_1L_{S0}}=\hat{M}$, $\dfrac{r_1\theta}{L_{S0}}=\hat{\theta}$, $\dfrac{n_2}{n_1}=n_0$, $\dfrac{K_S}{K_r}=K_0$, $\dfrac{a}{L_{S0}}=a_0$, $\dfrac{b}{L_{S0}}=b_0$, $\dfrac{r_2}{r_1}=r_0$, $\dfrac{\delta}{L_{S0}}=\delta_0$, $1=a_0-b_0+\delta_0$. Where n_1 represents the number of flexible rods, n_2 represents the numbers of springs, K_S represents the spring stiffness, K_r represents torsional stiffness of flexible rods, a represents the total length of connecting rods and springs when they are in a state of static equilibrium, b represents the length of connecting rod, r_1 represents the radial displacement of positive stiffness element, and r_2 represents the radial displacement of negative stiffness element.

Therefore, Eq.(9) can be recast in non-dimensional form as

$$\hat{M} = \hat{\theta} - 2n_0K_0r_0^2\hat{\theta}\left[\frac{1-a_0}{\sqrt{b_0^2-(r_0\hat{\theta})^2}}+1\right] \tag{10}$$

We differentiate Eq.(10) with respect to the non-dimensional degree $\hat{\theta}$ in order to determine the stiffness $\hat{K}$.

$$\hat{K} = 1 - \hat{k}_0\left[\frac{(1-a_0)\cdot b_0^2}{\left(b_0^2-(r_0\hat{\theta})^2\right)^{\frac{3}{2}}}+1\right] \tag{11}$$

where $\hat{k}_0 = 2n_0K_0r_0^2$

The basic dimensions and parameters of the calculation model of vibration isolator in this paper are shown in Tab.1.

Tab.1 Dimensions and parameters of vibration isolator

Symbol	Units	Value	Symbol	Units	Value
n_1	–	3	b	mm	92
n_2	–	3	L	mm	70
K_S	N·mm	21.33	L_{so}	mm	65
K_r	N·mm · rad^{-1}	41.58	r_1	mm	24
a	mm	135	r_2	mm	50

Fig. 4 shows the relationship between the dimensionless recovery torque, spring pre-compressed deformation and angular displacement drawn by Eq.(10). It can be seen from the figure that there is a nonlinear relationship between the angular displacement and the recovery torque. Fig.5 shows the relationship between the dimensionless stiffness and the spring pre-compressed deformation and angular displacement drawn by Eq.(11). The figure illustrates that the vibration isolator exhibits quasi-zero stiffness characteristics when a certain value of angular displacement and spring pre-compressed deformation is reached.

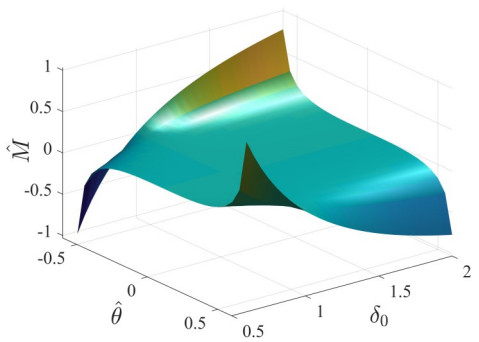

Fig.4 Relationship between dimensionless restoring torque and spring pre-compressed deformation and angular displacement

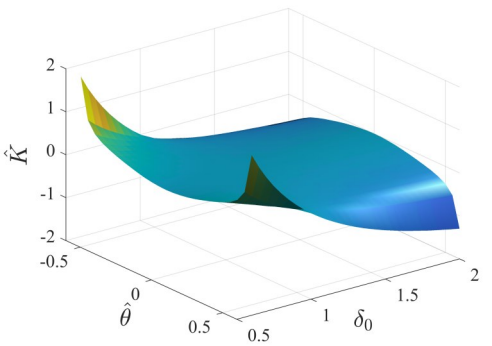

Fig. 5 Relationship between dimensionless stiffness and spring pre-compressed deformation and angular displacement

2.2 Simulated and experimental analysis of quasi-zero stiffness characteristics of HSLDS torsional vibration isolators

To validate the HSLD stiffness characteristics of the proposed vibration isolator, ANSYS Workbench software was utilized to simulate both negative and positive stiffness structures separately. The dimensions and parameters of the FEM model are given in Tab.1. The simulation results are shown in Fig.7. It can be seen from the figure that the vibration isolator exhibits quasi-zero stiffness characteristics for specific structural parameters.

To validate the accuracy of simulation results, a static torque load test was conducted on the 3D printed model of the proposed vibration isolator using WNJ-200 torsion testing machine. The test results were then compared with theoretical simulation outcomes. The dimensions and parameters of the 3D printed model for the vibration isolator are presented in Tab.1. WNJ-200 torsion testing machine is composed of computer control unit, torque detection unit, torsion angle detection unit

and motor system unit. The torsion test of HSLDS vibration isolator is shown in Fig.6.

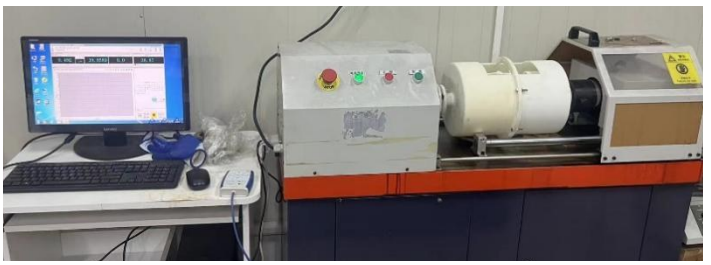

Fig.6 Torsion test of HSLDS vibration isolator

During the experiment, one end of the testing machine was fixed while the other end was subjected to a constant angular velocity of 0.5° per minute. The comparison between the stiffness characteristic curves obtained from test and simulation results is presented in Fig. 7. The test indicates that the vibration isolator exhibits nonlinearity in simulation, thereby validating the proposed torsional vibration isolator′s HSLD stiffness characteristics.

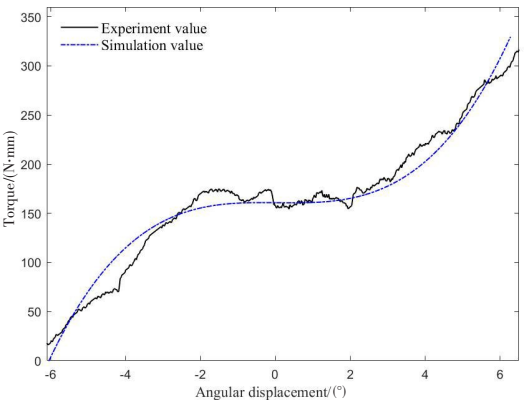

Fig.7 Stiffness curves of both experimental testing and simulation analysis

3 Analysis of torque transfer characteristics of HSLDS torsional vibration isolators affected by the isolators' parameters

If the dimensionless restoring moment $\hat{M}$ obtained from Eq.(10) is expanded by Taylor formula expansion at $\theta = 0$, then its first 2 steps expression can be given by

$$\hat{M} = \hat{M} = \left[\hat{K}\left(\frac{a_0 - 1}{b_0} - 1\right) + 1\right]\hat{\theta} + \hat{K}\frac{a_0 - 1}{2{b_0}^3}\hat{\theta}^3 = \hat{k}_1\hat{\theta} + \hat{k}_3\hat{\theta}^3 \tag{12}$$

where, $\hat{k}_1 = \left[\hat{K}\left(\frac{a_0 - 1}{b_0} - 1\right) + 1\right]$, $\hat{k}_3 = \hat{K}\frac{a_0 - 1}{2{b_0}^3}$

When the vibration isolation system is in a state of static equilibrium and subjected to cosine excitation with an amplitude of M_e from the input point, the torque equation of the system can be expressed as follows:

$$J\theta'' + C\theta' + M = M_e\cos(\omega t) \tag{13}$$

While the propeller serves as both the input point subjected to torque excitation and the response point of the vibration isolation system, Eq.(13) can be nondimensionalized by introducing the following constants and variables:

$$\frac{n_1 K_r r_1^2}{J} = \omega_n^2,\ \frac{C}{2J\omega_n} = \xi,\ \frac{\omega}{\omega_n} = \Omega,\ \omega_n t = \tau,\ \frac{M_e r_1}{JL^2{}_{SO}\omega_n^2} = \hat{M}_e$$

where, J denotes the moment of inertia, C denotes the damping coefficient, ξ denotes the damping ratio, ω denotes the excitation frequency, ω_n denotes the natural frequency, and τ denotes non-di-

mensional time. Based on those dimensionless constants and variables above, Eq.(13) can be rewritten as non-dimensional form:

$$\hat{\theta}'' + 2\xi\hat{\theta}' + \hat{M} = \hat{M}_e\cos(\Omega\tau) \tag{14}$$

Substituting Eq.(12) into Eq.(14), we can get the equation as follows:

$$\hat{\theta}'' + 2\xi\hat{\theta}' + \hat{k}_1\hat{\theta} + \hat{k}_3\hat{\theta}^3 = \hat{M}_e\cos(\Omega\tau) \tag{15}$$

Supposing the response solution of Eq.(15) is $\hat{\theta} = \hat{\theta}_f \cdot \cos(\Omega\tau + \psi_f)$, an approximate solution can be obtained by using harmonic balance method. By ignoring the higher harmonic terms and eliminating the different phase, the amplitude frequency response equation can be gained as

$$\left(-\Omega^2\hat{\theta}_f + \hat{k}_1\hat{\theta}_f + \frac{3\hat{k}_3\hat{\theta}^3{}_f}{4}\right)^2 + \left(-2\xi\Omega\hat{\theta}_f\right)^2 = \hat{M}_e^2 \tag{16}$$

The torque transmitted from the propeller to the driven shaft can be given as follows:

$$\hat{M}_t = 2\xi\hat{\theta}' + \hat{k}_1\hat{\theta} + \hat{k}_3\hat{\theta}^3 \tag{17}$$

Since the phase difference between elastic torque and damping torque is 90°, the torque transmissibility of the isolation system is given as follows:

$$T = 20\lg\left(\frac{|\hat{M}_t|}{\hat{M}_e}\right) = 20\lg\left[\sqrt{\left(-2\xi\Omega\hat{\theta}_f\right)^2 + \left(\hat{k}_1\hat{\theta}_f + \frac{3\hat{k}_3\hat{\theta}^3{}_f}{4}\right)^2} \Big/ \hat{M}_e\right] \tag{18}$$

3.1 Effects of stiffness ratio, damping ratio, and excitation amplitude term on torque transmissibility

The effect of stiffness ratio $\hat{k}_3$ on torque transmissibility is shown in Fig.8. When the damping ratio ξ is set to 0.08, excitation amplitude $\hat{M}_e$ is set to 1, and stiffness ratio $\hat{k}_3$ gradually increases from 0.2 to 5, the peak value of the torque transmissibility gradually increases. It can be seen that the resonant frequency increases accordingly as the stiffness ratio is increased. However, the torque transmissibility remains the same in the high frequencies regardless of different stiffness ratios and the isolation frequency band is reduced.

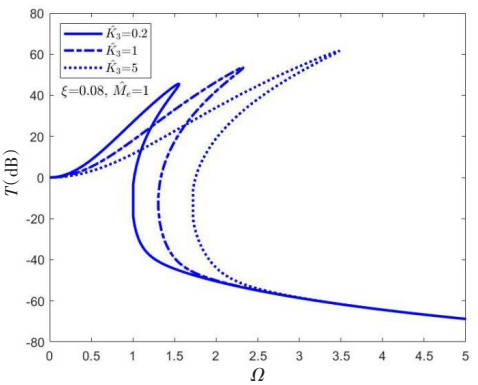

Fig.8 Torque transmissibility affected by different stiffness ratios of $\hat{k}_3$

The effect of damping ratio ξ on torque transmissibility is illustrated in Fig.9. When the stiffness ratio $\hat{k}_3$ is set to 1, excitation amplitude $\hat{M}_e$ is set to 1, and the damping ratio ξ gradually increases from 0.04 to 0.2, the peak value of the torque transmissibility decreases. The resonant frequency and the peak value of the torque transmissibility are decreased as the damping ratio is increased. However, the torque transmissibility increases in the high frequency region, which means the vibration attenuation becomes worse with the damping ratio increased. The conclusion can be obtained that damping degrades the efficiency of vibration isolation in high frequency domain just like the linear system.

The effect of excitation amplitude $\hat{M}_e$ on torque transmissibility is shown in Fig.10. When the

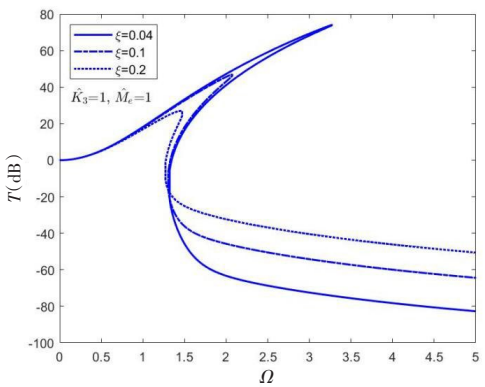

Fig.9 Torque transmissibility affected by different damper ratios of ξ

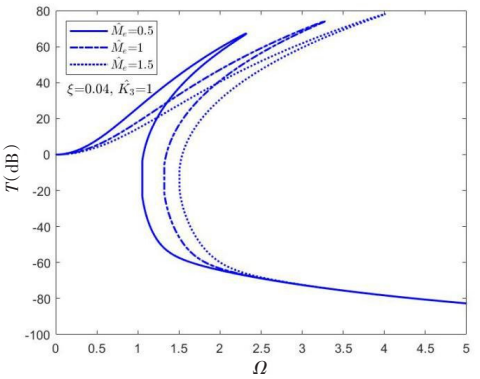

Fig.10 Torque transmissibility affected by different excitation amplitudes of $\hat{M}_e$

damping ratio ξ is set to 0.04, and stiffness ratio $\hat{k}_3$ is set to 1 , and the excitation amplitude $\hat{M}_e$ increases from 0.5 to 1.5, the peak value of the torque transmissibility increases. It can be clearly observed that the resonant frequency increases as the excitation torque is increased and the isolation frequency band is reduced. Moreover, increasing the excitation torque has little effect on the isolation performance in the high frequency region.

3.2 Comparison of torque transmissibility of an HSLDS vibration isolator and a typical linear isolator

When $\hat{k}_1$ is set to 1 and $\hat{k}_3$ to 0, indicating that the HSLDS isolator possesses solely positive stiffness elements, the system can be deemed a linear vibration isolator. The torque transmissibility can be determined by utilizing Eq.(15) as follows:

$$T_L = \frac{\sqrt{\left(-2\xi\Omega\right)^2 + 1}}{\sqrt{(1-\Omega^2)^2 + \left(2\xi\Omega\right)^2}} \tag{19}$$

When the damping ratio ξ is 0.04 and excitation $\hat{M}_e$ is 0.1, the comparison of torque transmissibility of an HSLDS isolator and a linear isolator is shown in Fig.11. The HSLDS isolator exhibits a lower initial frequency and a wider vibration isolation range, resulting in superior low-frequency vibration isolation performance compared to a linear isolator.

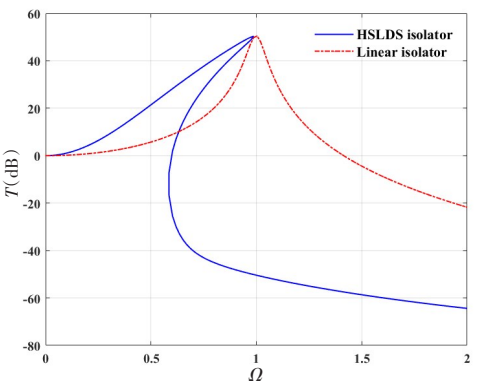

Fig.11 Comparison of torque transmissibility between HSLDS vibration isolator and linear vibration isolator

4 Numerical simulation of dynamic responses of HSLDS vibration isolator and linear isolator

The non-dimensional dynamic Eq.(15) is numerically simulated using fourth-order Runge-Kutta methods to calculate the system's dynamic response. Fig.12 displays the dynamic response curves of the HSLDS isolator system under harmonic excitation at a frequency of 4 Hz, with an exci-

tation torque amplitude set to 0.1. It can be seen that the response amplitude of the HSLDS isolator is smaller than that of the linear isolator under harmonic excitation. Nevertheless, root mean square (RMS) values of the non-dimensional moment are depicted in Fig.13 corresponding to Fig.12. It can be observed that RMS value responses of the HSLDS isolator is 0.032, which is smaller than that of linear isolator and base excitation. In special working conditions such as acceleration, deceleration, and flight of marine engine, the propeller blades will experience multiple frequency superimposed pulsating excitation in the fluid. Therefore, to investigate the response of the isolator under multi-frequency harmonic and shock excitations, a simulation of multi-frequency excitation was conducted by superimposing different harmonic excitations. The torque expression for multi-frequency harmonic excitation is presented in Eq.(20). The shock excitation simulation is configured as a half-sine wave with a pulse duration of 1 second and an excitation amplitude of 0.1, where the torque expression for shock excitation is presented in Eq.(21). In practical engineering applications, the damping ratio is typically determined by four factors: (1) material damping, which is the primary source of energy dissipation; (2) damping due to the surrounding medium; (3) damping at joints and support connections; and (4) loss of energy through the supporting foundation. Generally the damping ratio of the vibration system is typically specified within the range of 0.01 and 0.7. Here we set the damping ratio to be 0.2 for all simulations presented in this paper.

$$\hat{M}_a = 0.15\sin(4\pi t) + 0.13\sin(3.2\pi t) + 0.11\sin(1.6\pi t) + 0.08\sin(2.2\pi t) \tag{20}$$

$$\hat{M}_b = 0.1\sin(\pi t) \tag{21}$$

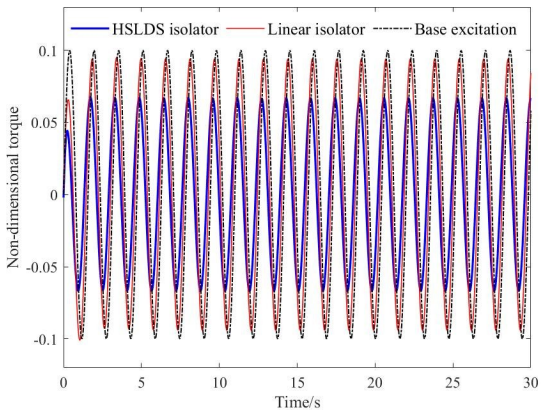

Fig.12 Responses of non-dimensional torque under harmonic excitation at frequency of 4 Hz

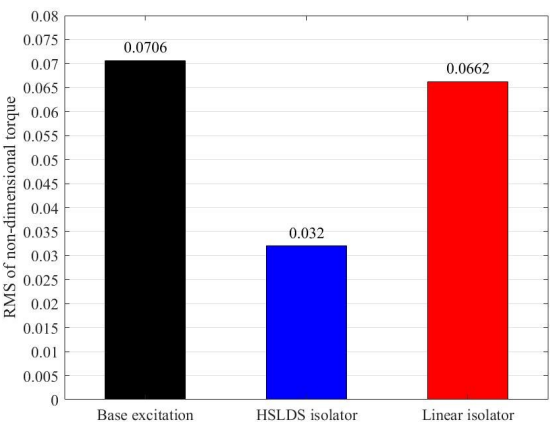

Fig.13 RMS values of the non-dimensional torque

The dynamic response curves under multi-frequency harmonic excitation of torque are shown in Fig.14, which can be observed that the dynamic response amplitude of the HSLDS isolator is significantly lower than that of the linear isolator and base excitation. Fig.15 demonstrates that the response amplitude of the HSLDS isolator can effectively reduce the base excitation amplitude within a short period, whereas the linear isolator requires more time to diminish torque amplitude, indicating that the HSLDS isolator is capable of promptly isolating shock and attenuating residual vibration. Therefore, the isolation performance of an HSLDS isolator for torsional vibration is significantly superior to that of a linear isolator.

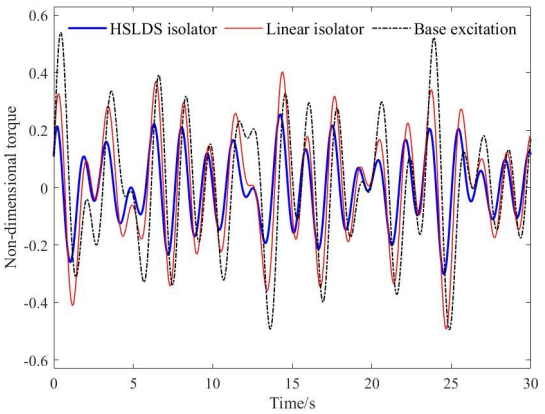

Fig.14 Non-dimensional torque responses under multi-frequency excitation

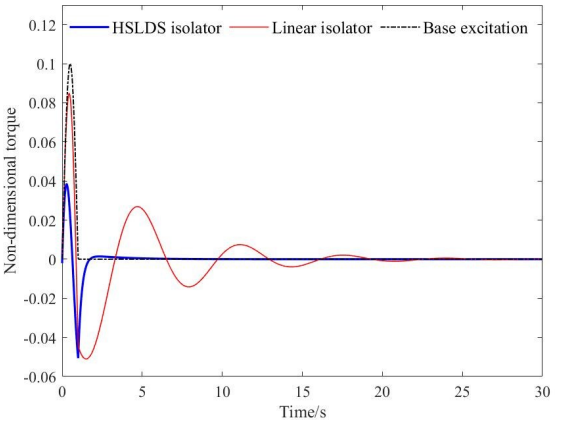

Fig.15 Non-dimensional torque responses under shock excitation

5 Experimental investigation

5.1 Experimental setup of HSLDS torsional vibration isolator

The experimental setup of an HSLDS torsional vibration isolator is shown in Fig.16. The harmonic excitation was generated by a shaker (JZ-10) with an excitation frequency ranging from 1-25 Hz and an excitation force amplitude of 0.5 N, which was driven by an arbitrary waveform generator (AFG1022) through a power amplifier (GF-100). Furthermore, the shaker applied a force to the rod extending radially along the input end of propeller shaft to generate torsional harmonic excitation amplitude of 50 N·mm. The HSLDS torsional vibration isolator was installed between the input and output ends of the ship′s shafting. Two dynamic torque sensors were installed on the propeller (input point) and driven shaft (output point). The dynamic signal analysis system (DH5922) utilized embedded signal processing software (DHDAS) to analyze data collected from two JN-DN3 sensors.

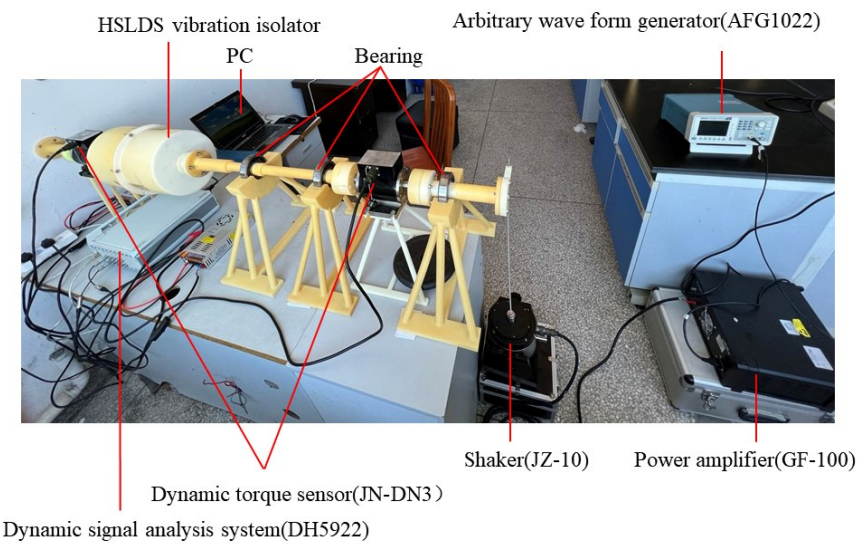

Fig.16 Experimental platform of HSLDS vibration isolator

5.2 Experimental results

The dynamic torques of two ends of the shaft were collected respectively by two dynamic

torque sensors. The vibration isolation performance could be defined as the reduction of vibrations between the HSLDS vibration isolator and linear vibration isolator. The reduction of vibration was achieved by multiplying the logarithm of the ratio between the output and input torques from two sensors by a factor of 20. The experimental results are illustrated in Fig.17, indicating that the vibration reduction of HSLDS vibration isolator surpasses that of linear vibration isolator. This confirms its superior performance in terms of vibration isolation.

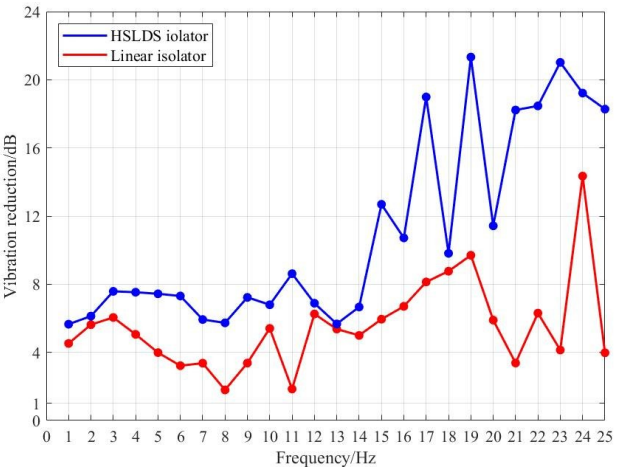

Fig.17 Experimental results of HSLDS vibration isolator and linear vibration isolator

6 Conclusions

This paper presents the development of the geometric and mechanical models of an HSLDS torsional vibration isolator, which comprises a negative stiffness structure in the form of a connecting rod spring and a parallel positive stiffness structure consisting of circular section flexible rods. The FEM analysis, numerical simulation analysis, and experimental analysis of 3D printed physical objects were conducted. The research findings demonstrate that the torsional vibration isolator exhibits high-static-low-dynamic stiffness characteristics in the torsion direction, while also possessing significant axial load-carrying capacity for static torque. To enhance the vibration isolation performance of an HSLDS isolator, it is possible to reduce the stiffness ratio $\hat{k}_3$ by adjusting the dimensions of a_0 and b_0 of both the connecting rod and the spring mechanism. Additionally, reducing the damping ratio ξ can also improve the vibration isolation performance of the vibration isolator. Moreover, the HSLDS torsional vibration isolator exhibits a lower starting frequency for vibration isolation compared to its linear counterpart and boasts a wider range of frequencies for effective isolation. As such, it delivers superior performance in attenuating low-frequency vibrations.

References

[1] Qi L B, Wu Y S, Zou M S, et al. Propeller-shaft-hull coupled vibration and its impact on acoustic radiation utilizing sono-elasticity theory[J]. Ocean Engineering, 2019, 171: 391-398.

[2] Murawski L, Dereszewski M. Theoretical and practical backgrounds of monitoring system of ship power transmission systems′ torsional vibration[J]. Journal of Marine Science and Technology, 2020, 25: 272-284.

[3] Xie X L, Yang D Q, Wu D, et al. Theoretical analysis on vibration transmission control in a shaft-hull system excited by propeller forces via an active multi-strut assembly[J]. Ocean Engineering, 2021, 221: 108544.

[4] Li X Y, Zhang M L. Mechanical vibration[M]. Beijing: Tsinghua University Press, 2009. (in Chinese)

[5] Zhang F, Xu M L, Shao S B, et al. A new high-static-low-dynamic stiffness vibration isolator based on magnetic negative stiffness mechanism employing variable reluctance stress[J]. Journal of Sound and Vibration, 2020, 476: 115322.

[6] Yao Y H, Li H G, Li Y, et al. Analytical and experimental investigation of a high-static-low-dynamic stiffness isolator with cam-roller-spring mechanism[J]. International Journal of Mechanical Sciences, 2020, 186: 105888.

[7] Zheng Y S, Zhang X N, Luo Y J, et al. Analytical study of a quasi-zero stiffness coupling using a torsion magnetic spring with negative stiffness[J]. Mechanical Systems and Signal Processing, 2018, 100: 135-151.

[8] Zhang C S, Li X Y, Zhang S, et al. Design and analysis of quasi-zero stiffness torsional vibration isolator adapting to load changes[J]. Journal of Vibration and Shock, 2022, 41(23): 307-314. (in Chinese)

[9] Zhang C, He J, Zhou G Q, et al. Compliant quasi-zero-stiffness isolator for low-frequency torsional vibration[J]. Mechanism and Machine Theory, 2023, 181: 105213.

[10] Zhou J X, Xu D L, Bishop S. A torsion quasi-zero stiffness vibration isolator[J]. Journal of Sound and Vibration, 2015, 338: 121-133.

[11] Wang K, Zhou J X, Xu D L. Sensitivity analysis of parametric errors on the performance of a torsion quasi-zero-stiffness vibration isolator[J]. International Journal of Mechanical Sciences, 2017, 134: 336-346.

[12] Liu H, Wang X J, Xiang C L. Analysis and experimental study on the dynamic characteristics of a torsional vibration damper with negative stiffness structure[J]. Automotive Engineering, 2016, 38(12): 1483-1487. (in Chinese)

[13] Wang X J, Liu H, Li W P, et al. Vibration transmission characteristics of a quasi-zero-stiffness torsional isolator[J]. Journal of Mechanical Engineering, 2018, 54(21): 49-56. (in Chinese)

船舶轴系高静低动扭振隔振装置理论及试验研究

李林桃[1], 卢佳钟[1], 杨志荣[1], 肖望强[2], 饶柱石[3]

(1. 集美大学 轮机工程学院 福建 厦门 361021; 2. 厦门大学 航空航天学院, 福建 厦门 361000;
3. 上海交通大学 机械系统与振动全国重点实验室, 上海 200240)

摘要: 具有高静低动刚度特性的隔振器是一种有效的低频隔振方式,可用于船舶轴系的低频扭振隔振。本文通过并联正刚度和负刚度元件,设计一种机构紧凑的高静低动刚度扭振隔振装置;通过力学模型分析,分别推导负刚度构件中弹簧和连杆的回复力矩,以及正刚度构件中圆截面柔性杆的回复力矩;通过对模型进行静力学仿真和试验得到扭振隔振装置的准零刚度特性曲线;通过数值模拟仿真分析和扭矩传递特性理论分析,评估扭转隔振性能;最后,进行了动态扫频激振试验。试验结果表明,高静低动扭振隔振装置相比线性隔振装置具有更好的低频隔振性能,是针对船舶轴系低频扭转振动可供借鉴的解决方案。

关键词: 船舶轴系; 高静低动刚度; 扭振隔振装置

中图分类号: U664.21 **文献标识码:** A

基金项目: 国家自然科学基金面上项目(52475104); 福建省科技计划引导性项目(2024H0015); 福建省高校产学研联合创新项目(2022H6003); 中核集团领创科研项目(22GFC-JJ12-475)

作者简介: 李林桃(1996-),男,硕士研究生;
杨志荣(1981-),男,博士,集美大学副教授。